

Local Electronic Structure around a Single Kondo Impurity

Patrick Huang and Emily A. Carter*

Department of Mechanical & Aerospace Engineering and Program in Applied & Computational Mathematics, Princeton University, Princeton, New Jersey 08544-5263

Received February 7, 2006; Revised Manuscript Received March 7, 2006

ABSTRACT

The local electronic structure due to the adsorption of Co on Cu(111) is studied using an embedded cluster model, in which the crystal background is taken into account via an effective density functional theory (DFT)-based potential. This approach goes beyond the usual single-impurity Anderson model, where the ground state consists of a singly occupied impurity whose moment is compensated by the background conduction electrons. Ab initio correlated wave function calculations for the embedded cluster provide an alternative picture for this ground state and indicate that the quenching of the Co magnetic moment is due to the formation of metal–metal bonds with the Cu substrate. Low-lying excitations are also studied within the embedding model, and our results are discussed in the context of scanning tunneling microscopy experiments (Manoharan, H. C.; Lutz, C. P.; Eigler, D. M. *Nature* 2000, 403, 512), which find a sharp tunneling resonance localized in the vicinity of the Co adatom.

The coupling between a localized spin and its environment is a general problem of fundamental interest and arises in a number of physical situations. One important example is the well-known “Kondo effect”, which was originally studied in the context of a magnetic impurity atom embedded in a bulk, nonmagnetic metal. In the Kondo theory,¹ the coupling between the impurity moment and the continuum of conduction states leads to a many-body open-shell singlet ground state, with the conduction electron spins aligned to screen out the impurity moment. Below a temperature T_K , the formation of this Kondo ground state is signaled by the appearance of a sharp resonance in the density of states at the Fermi energy ϵ_F , whose width is on the order of $k_B T_K$.

As a result of recent advances in sophisticated experimental techniques to manipulate matter at atomic length scales, it is now possible to directly probe the Kondo effect due to individual spin moments. Within the past decade, a variety of nanoscale systems have been shown to exhibit Kondo-like physics. In the case where the localized moment is due to a transition metal d or f electron, the background of continuum states can be provided by metallic surfaces^{2–4} or carbon nanotubes.⁵ Single-molecule analogues such as cerocene,^{6–8} thorocene,⁷ and ytterbocene⁸ have also been studied, in which the f electrons on the rare-earth atoms are believed to be singlet-coupled to planar aromatic ligands. Gated structures involving two metallic electrodes bridged by organometallic complexes,^{9–12} carbon nanotubes,¹³ or C_{60} molecules¹⁴ also demonstrate characteristic Kondo behavior and offer the possibility of novel spintronic devices which exploit Kondo physics.

In this Letter, we shall consider the case of a single magnetic adatom adsorbed on a nonmagnetic, metallic surface, namely, Co on the (111) surface of Cu.^{4,15} This is one of the first systems where the Kondo effect due to an individual spin moment was unambiguously observed at atomic length scales. Scanning tunneling microscopy (STM) experiments of magnetic, first-row transition metal adatoms on noble metal (111) surfaces reveal a narrow (~ 0.01 eV width) resonance in the density of states near ϵ_F , localized within a range of ~ 10 – 60 Å from the adatom. The sharp resonance at ϵ_F was taken as a direct signature of the Kondo ground state, localized within the vicinity of the magnetic adatom. Its line shape can be modeled as a Fano-type interference between two tunneling channels: direct tunneling between the STM tip and the adatom, and tunneling between the STM tip and the conduction states of the substrate, modified by the presence of the adatom.

Most theoretical interpretations of the STM experiments so far have been made within the framework of a single-impurity Anderson model.^{2,3,16,17} In the localized moment regime, the mean-field ground state of the Anderson model consists of a singly occupied impurity coupled to a background of continuum states, while empty or doubly occupied impurity states appear in higher-lying excited Slater determinants. The many-body ground state is typically arrived at by first mapping this Anderson model onto an effective Kondo model via the Schrieffer–Wolff transformation,¹⁸ a procedure which constrains the impurity level to be singly occupied.

In this work, we report ab initio, correlated many-body wave function calculations that provide an alternative view

* To whom correspondence may be addressed. E-mail: eac@princeton.edu.

of the character of the Kondo resonance. Namely, these calculations suggest that the impurity moment quenching is due to formation of chemical bonds involving the impurity d electrons and the s electrons from the nearest-neighbor atoms of the substrate. We employ a density-based embedding strategy suitable for periodic bulk crystals, which has been described in detail in earlier papers.^{19–21} In short, the approach begins by partitioning the total system density ρ into an embedded cluster ρ_I and background ρ_{II} . The total energy $E[\rho]$ is regarded as $E[\rho] = E_I[\rho_I] + E_{II}[\rho_{II}] + E_{\text{int}}$, where E_I and E_{II} represent the embedded cluster and background energies, respectively. E_{int} is the cluster-background interaction energy, defined as $E_{\text{int}} = E[\rho] - E_I[\rho_I] - E_{II}[\rho_{II}]$.

Since $\rho = \rho_I + \rho_{II}$, we choose the independent variables to be ρ and ρ_I . Assuming the background region is large enough such that $\delta E_{II}/\delta \rho_I \approx 0$, variation of $E[\rho]$ with respect to ρ and ρ_I leads to the Euler equations

$$\frac{\delta E}{\delta \rho} = 0 \quad (1)$$

$$\frac{\delta E_I}{\delta \rho_I} + v_{\text{emb}} = 0 \quad (2)$$

The first equation above can be solved via a standard application of Kohn–Sham density functional theory (DFT)²² to yield the total crystal density ρ . The second equation involves just the cluster alone, in the presence of an effective embedding potential v_{emb} representing the background. The potential v_{emb} is given by $v_{\text{emb}} = v_{T_s} + v_J + v_{x_c} + v_{\text{ion}}$, where

$$v_{T_s} = \frac{\delta T_s[\rho]}{\delta \rho} - \frac{\delta T_s[\rho_I]}{\delta \rho_I} \quad (3)$$

$$v_J = \frac{\delta J[\rho]}{\delta \rho} - \frac{\delta J[\rho_I]}{\delta \rho_I} \quad (4)$$

$$v_{x_c} = \frac{\delta E_{x_c}[\rho]}{\delta \rho} - \frac{\delta E_{x_c}[\rho_I]}{\delta \rho_I} \quad (5)$$

$$v_{\text{ion}} = v_{\text{ion}}^{\text{II}} \quad (6)$$

The functionals T_s , J , and E_{x_c} are the usual DFT noninteracting kinetic energy, Hartree, and exchange correlation contributions, respectively. $v_{\text{ion}}^{\text{II}}$ is the ion–electron interaction due to the background ions. Details on the evaluation of these terms are given in refs 19–21.

We begin with a plane-wave DFT calculation for the Co/Cu(111) system, where the plane-wave basis set was truncated at a kinetic energy cutoff value of 800 eV. We use the local spin density approximation (LSDA) of Perdew and Zunger for exchange correlation.²³ The Cu and Co atoms are modeled using Vanderbilt ultrasoft pseudopotentials²⁴ derived from the local density approximation (LDA), with 11 and 9 valence electrons for each Cu and Co atom,

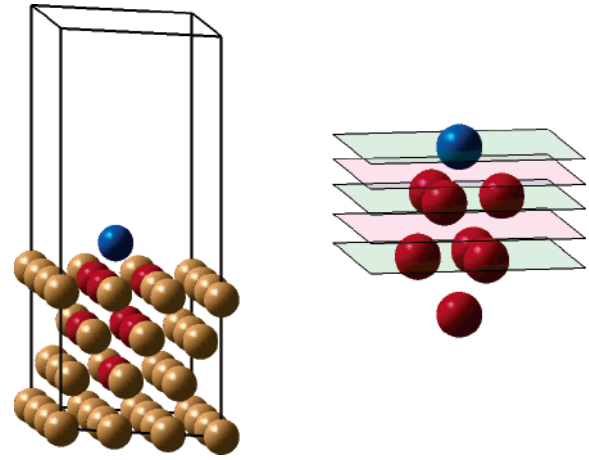


Figure 1. Periodic DFT supercell geometry (left), and embedded CoCu₇ cluster (right). The Co atom is shown in blue, the embedded Cu atoms in red, and the background Cu atoms in gold. The slice planes indicate cuts along which the three-dimensional orbitals are drawn in Figure 2.

respectively. The total system supercell (Figure 1) consists of a four-layer, Cu(111) slab with 9 Cu atoms per layer, and a bulk lattice parameter of 3.57 Å. This value corresponds to the equilibrium bulk face-centered cubic (fcc) Cu lattice parameter associated with our Cu pseudopotential. A single Co atom is placed in a 3-fold fcc hollow site, which is the minimum energy site. Brillouin zone integrations were performed on a $5 \times 5 \times 1$ Monkhorst–Pack k -point mesh,²⁵ symmetrized to give five irreducible k -points. The positions of the Co and the top two layers of Cu were allowed to relax until the magnitudes of all forces acting on these atoms were less than 0.05 eV/Å. All plane-wave DFT calculations were performed using the CASTEP code.²²

In the opposite regime, we also examine bare clusters of CoCu_{*n*} ($n = 3, 7$) removed from the periodic Co/Cu(111) slab; i.e., the cluster atom positions are taken from the Co/Cu(111) optimized geometry. The CoCu₃ cluster consists of Co and the three nearest-neighbor Cu atoms of the 3-fold fcc hollow site, while the CoCu₇ cluster includes three additional Cu atoms from the second layer and one Cu atom from the third layer (Figure 1). DFT calculations were performed for these bare clusters using the same LDA pseudopotentials as those used for bulk Co/Cu(111), within a supercell where the cluster centers are separated from their periodic images by ~ 15 Å.

In both the bare cluster and bulk cases studied here at the spin-polarized DFT level, we find a ground state with a net magnetic moment of $\sim 2 \mu_B$ localized on the Co adatom (Table 1). While some spin density can be seen on neighboring Cu atoms in the case of the smallest cluster, CoCu₃, this vanishes in the bulk limit. The bulk picture here is consistent with a mean-field treatment of the Anderson model in the local moment regime, as opposed to a spin-compensated ground state expected when electron correlations are properly taken into account. This discrepancy can be attributed to the use of approximate exchange-correlation functionals, which are not guaranteed to capture all important electron correlation effects.

Table 1. DFT Magnetic Moments (μ_B) for Bare CoCu_n ($n = 3, 7$), and the Bulk Co/Cu(111) Slab^a

	Co	Cu layer-1 n.n.	Cu layer-2 n.n.
bare CoCu_3	1.76	-0.28	
bare CoCu_7	2.32	0.10	0.12
bulk Co/Cu(111)	2.08	-0.04	0.0

^a The heading “layer-1 n.n.” refers to the nearest-neighbor Cu atoms in the fcc hollow site upon which the Co adatom resides, and “layer-2 n.n.” denotes the nearest-neighbor Cu atoms in the layer below.

Ab initio configuration interaction (CI) electron correlation calculations for CoCu_n permit us to go beyond the limitations of approximate DFT functionals and provide insight into excited states. All CI calculations were done within the MOLCAS program package.²⁶ We utilize Hay-Wadt large-core pseudopotentials derived from Hartree–Fock theory and their corresponding optimized basis sets.²⁷ The CI studies begin with the complete active space, self-consistent field (CASSCF) method,²⁸ which is a full CI calculation within some prespecified orbital subspace (“active space”). For CoCu_3 , this subspace is spanned by the Co 3d4s and Cu 4s orbitals, to give 12 valence electrons distributed over 9 active orbitals, i.e., a CAS(12/9) calculation. The 15 Cu 3d orbitals are assumed to be doubly occupied (inactive). The active space for CoCu_7 is chosen similarly, except that two valence electrons are assumed to doubly occupy an inactive orbital formed from a totally symmetric combination of all 4s orbitals, resulting in a CAS(14/9) calculation.

The initial CASSCF calculations are subsequently followed by multireference singles and doubles CI (MRSDCI),²⁹ in which all single and double excitations out of some pre-specified set of reference configurations are included in the CI expansion. For CoCu_n , the optimized orbital basis set is taken from the preceding CASSCF calculation, and the resulting configurations whose CI coefficients have a magnitude ≥ 0.05 are used as references for the MRSDCI. Again, the subspace spanned by the Cu 3d orbitals (15 for CoCu_3 and 35 for CoCu_7) are frozen, i.e., they are doubly occupied in all configurations of the CI expansion, leaving 12 explicitly correlated electrons for CoCu_3 and 16 for CoCu_7 .

To model the effect of the periodic crystal, we apply the embedding approach discussed earlier. Correlations between electrons in the embedded cluster are explicitly treated with CI, while the background is described at the DFT level via the effective embedding potential v_{emb} of eqs 3–6. In general, the exact functional dependence of the kinetic energy T_s and exchange-correlation E_{xc} are not known, and thus the construction of v_{emb} begins with a choice for the form of T_s and E_{xc} . We approximate these terms using the Thomas–Fermi 1/9–von Weizsäcker functional for T_s , and the LDA form for E_{xc} is chosen for consistency with the plane-wave DFT calculations. Next, an estimate for the background density is obtained as $\rho_{\text{II}} = \rho - \rho_{\text{I}}^{\text{bare}}$, where ρ is the DFT density for the Co/Cu(111) slab, and $\rho_{\text{I}}^{\text{bare}}$ is the DFT density for the bare CoCu_n ($n = 3, 7$) cluster. This background density ρ_{II} is regarded as fixed in our embedding model.

An initial guess for v_{emb} is obtained by first evaluating eqs 3–6 with ρ taken from the plane-wave DFT calculation

Table 2. Low-Lying States of the CoCu_3 Cluster^a

term	CAS(12/9) (eV)	MRSDCI (eV)
$^3\text{A}_1$ (bare)	0.15	0.06
$^1\text{A}_1$	0.0	0.0
$^3\text{A}_1$ (embedded)	1.20	1.48
$^1\text{A}_1$	0.0	0.0

^a The upper entries give the bare cluster results relative to the bare cluster $^1\text{A}_1$ ground state, while the lower entries give the embedded cluster results relative to the embedded cluster $^1\text{A}_1$ ground state.

Table 3. Low-Lying States of the CoCu_7 Cluster^a

term	CAS(14/9) (eV)	MRSDCI (eV)
^1E (bare)	0.85	0.65
^5E	0.60	0.28
^3E	0.08	0.12
$^3\text{A}_1$	0.05	0.09
$^3\text{A}_2$	0.0	0.0
^1E (embedded)	0.38	0.34
^5E	0.19	0.29
$^3\text{A}_1$	0.17	0.24
$^1\text{A}_1$	0.0	0.0

^a The upper entries give the bare cluster results relative to the bare cluster $^3\text{A}_2$ ground state, while the lower entries give the embedded cluster results relative to the embedded cluster $^1\text{A}_1$ ground state.

for Co/Cu(111) , and $\rho_{\text{I}} = \rho_{\text{I}}^{\text{bare}}$. CASSCF calculations are then performed for the CoCu_n cluster embedded in this v_{emb} , to yield an updated cluster density ρ_{I}' , and a total system density $\rho' = \rho_{\text{I}}' + \rho_{\text{II}}$. This leads to an updated embedding potential v_{emb}' , and the cycle is repeated until self-consistency. MRSDCI calculations of the ground and excited states are subsequently performed for the embedded cluster using this converged, self-consistent potential, $v_{\text{emb}}'[\rho', \rho_{\text{I}}']$.

The CI results for the energetics of bare and embedded CoCu_n clusters are summarized in Tables 2 and 3. The ground state of bare CoCu_3 is a singlet ($^1\text{A}_1$), and we find that the effect of the embedding increases the singlet–triplet splitting by over 1 eV. However, as STM experiments have measured the Kondo resonance at distances up to 10 Å away from the adatom center,⁴ the CoCu_3 cluster is probably much too small to provide a good description of the local electronic structure around the Co adatom, and a frozen DFT background is not expected to account for the strong correlations outside the embedded cluster.

CI calculations for the larger CoCu_7 reveal qualitative differences from CoCu_3 . The bare CoCu_7 ground state is a triplet ($^3\text{A}_2$), and the lowest excitations are purely density fluctuations in nature; i.e., they have the same spin multiplicity as the ground state. A singlet ($^1\text{A}_1$) ground state only emerges when the embedding is included, and the lowest excitations now involve spin fluctuations, consistent with the single-impurity Anderson model in the local moment regime. The singlet–triplet splitting decreases by an order of magnitude from that seen in embedded CoCu_3 , and it is reasonable to assume that the singlet–triplet splitting will continue to decrease as the cluster size increases.

Further insight into the ground state of the embedded CoCu_7 cluster can be gained by analyzing the structure of

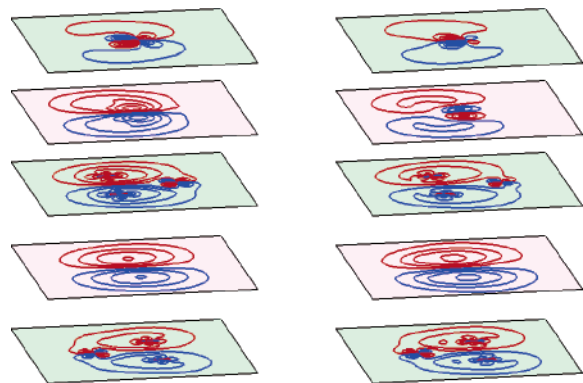


Figure 2. Embedded CoCu₇ cluster natural orbitals φ_{1e} (left) and φ_{2e} (right) for the 1A_1 ground state. Only one member of each doubly degenerate pair is shown. The contour slices are taken along the planes shown in Figure 1. Red contour lines indicate regions of positive amplitude, while blue denotes regions of negative amplitude.

Table 4. Multiconfigurational Character of the Embedded CoCu₇ Cluster Ground-State (1A_1) Wave Function^a

configuration	CI weight
$(\varphi_{1e})^2(\varphi_{1e'})^2$	0.43
$(\varphi_{1e})^2(\varphi_{2e'})^2 + (\varphi_{1e'})^2(\varphi_{2e})^2$	0.15
$(\varphi_{1e})^1(\bar{\varphi}_{1e})^1(\varphi_{2e})^1(\bar{\varphi}_{2e})^1$	0.14

^a Only configurations with CI weights greater than 0.1 are shown here.

the optimized CASSCF ground-state wave function. The strongest correlation effects are due to four electrons, distributed over two sets of doubly degenerate orbitals which transform as the e representation of the C_{3v} point group. We denote these orbitals as $\{\varphi_{1e}, \varphi_{1e'}\}$ and $\{\varphi_{2e}, \varphi_{2e'}\}$, and their contour plots are drawn in Figure 2. It can be seen that they are due to hybridization between the Cu atomic s orbitals and Co atomic d orbitals. The multiconfigurational character of the 1A_1 ground state is summarized in Table 4, which lists the important configurations present in the CI expansion. It is evident that the many-body ground state is a superposition of both open- and closed-shell configurations. Moreover, these configurations can be further analyzed to show that they consist of mixtures of configurations where each Co d orbital is empty, singly occupied, or doubly occupied, corresponding to the mixed valence regime of the Anderson model. A conventional treatment of the Anderson model, which assumes a singly occupied impurity (i.e., the local moment regime), provides only a partial picture of the true ground state. Instead, here we find that the quenching of the impurity moment is due to chemical bonds forming between the Co d orbitals and the nearest-neighbor Cu s orbitals.

While the embedding calculations provide a detailed description of the local ground state electronic structure near the Co adatom, a direct comparison with STM experiments is more difficult because our approach does not immediately yield a local density of states. The STM differential conductance dI/dV spectrum is due to tunneling between the probe and the substrate, i.e., transitions between N electron and $(N \pm 1)$ electron states. The measured dI/dV spectrum

Table 5. Mulliken Natural Orbital Populations of the Ground-State CoCu₇ MRSDCI Wave Functions^a

orbital	Co	Cu layer-1 n.n.	Cu layer-2 n.n.
s (bare)	0.58	1.17	1.10
d	7.96	10.02	10.02
s (embedded)	2.10	0.83	0.69
d	8.13	10.07	10.16

^a The upper entries correspond to the bare 3A_2 cluster, lower entries are the embedded 1A_1 cluster. The heading “layer-1 n.n.” refers to the nearest-neighbor Cu atoms in the fcc hollow site upon which the Co adatom resides, and “layer-2 n.n.” denotes the nearest-neighbor Cu atoms in the layer below.

for Co/Cu(111) shows a sharp Kondo resonance at about 0.001 eV above the Fermi level ϵ_F , which corresponds to tunneling of an electron from the STM tip to the substrate.⁴

We can gain some insight into this tunneling process by looking at Mulliken populations of the bare and embedded CoCu₇ cluster, shown in Table 5. While the d-orbital populations on Co and Cu are relatively unaffected by the embedding environment, the s-orbital population shifts toward the Co adatom, polarizing the cluster. The Co s states in the embedded cluster are essentially fully occupied, and it is not likely an additional electron will hop onto states localized on the Co. Thus, it is reasonable to conclude that an electron will preferentially tunnel into holelike s states on the neighboring Cu atoms. This is consistent with the STM work of ref 15, who made a detailed comparative study of Co on Cu(111) and Cu(001). From their analysis of the Kondo resonance line shape, they also concluded that tunneling onto Co/Cu(111) proceeds primarily into bulk substrate conduction states, not direct tunneling onto the Co adatom.

In summary, we have developed and investigated a DFT-based embedded cluster model for Co/Cu(111), in which the crystal background is represented as an effective potential acting on the cluster atoms of interest. Ab initio correlated wave function calculations for this embedded cluster yield a singlet ground state, consistent with the single-impurity Anderson model in the local moment regime. A careful examination of the many-body wave function reveals that the Co moment is quenched due to the formation of metal–metal bonds with the neighboring Cu atoms. This is in contrast to a mean-field, single-determinant Kohn–Sham DFT approach, which does not yield the correct spin-compensated ground state. A correlated wave function treatment of finite cluster models also fails to produce the correct singlet ground state, which can be attributed to the absence of an extended conduction band. Our work here provides an alternative interpretation of the STM data for Kondo impurities on metallic surfaces, which to date has primarily been analyzed within the framework of the Anderson model.

Acknowledgment. We thank Peter Nordlander, Niri Govind, and Thorsten Klüner for useful discussions, Accelrys, Inc., for providing the CASTEP code, and Roland Lindh for help with the MOLCAS code. This work was supported by a grant from the Department of Energy Basic Energy

Sciences. P.H. also acknowledges partial support from a California NanoSystems Institute postdoctoral fellowship.

References

- (1) Hewson, A. C. *The Kondo Problem to Heavy Fermions*; Cambridge Studies in Magnetism; Cambridge University Press: Cambridge, 1993.
- (2) Li, J.; Schneider, W.-D.; Berndt, R.; Delley, B. *Phys. Rev. Lett.* **1998**, *80*, 2893.
- (3) Madhavan, V.; Chen, W.; Jamneala, T.; Crommie, M. F.; Wingreen, N. S. *Science* **1998**, *280*, 567.
- (4) Manoharan, H. C.; Lutz, C. P.; Eigler, D. M. *Nature* **2000**, *403*, 512.
- (5) Odom, T. W.; Huang, J.-L.; Cheung, C. L.; Lieber, C. M. *Science* **2000**, *290*, 1549.
- (6) Dolg, M.; Fulde, P.; Küchle, W.; Neumann, C.-S.; Stoll, H. *J. Chem. Phys.* **1991**, *94*, 3011.
- (7) Dolg, M.; Fulde, P.; Stoll, H.; Preuss, H.; Chang, A.; Pitzer, R. M. *Chem. Phys.* **1995**, *195*, 71.
- (8) Booth, C. H.; Walter, M. D.; Daniel, M.; Lukens, W. W.; Andersen, R. A. *Phys. Rev. Lett.* **2005**, *95*, 267202.
- (9) Park, J.; Pasupathy, A. N.; Goldsmith, J. I.; Chang, C.; Yaish, Y.; Petta, J. R.; Rinkoski, M.; Sethna, J. P.; Abruña, H. D.; McEuen, P. L.; Ralph, D. C. *Nature* **2002**, *417*, 722.
- (10) Liang, W.; Shores, M. P.; Bockrath, M.; Long, J. R.; Park, H. *Nature* **2002**, *417*, 725.
- (11) Zhuang, M.; Rocheleau, P.; Ernerzhof, M. *J. Chem. Phys.* **2005**, *122*, 154705.
- (12) Liu, R.; Ke, S.-H.; Baranger, H. U.; Yang, W. *Nano Lett.* **2005**, *5*, 1959.
- (13) Nygård, J.; Cobden, D. H.; Lindelof, P. E. *Nature* **2000**, *408*, 342.
- (14) Yu, L. H.; Natelson, D. *Nano Lett.* **2004**, *4*, 79.
- (15) Knorr, N.; Schneider, M. A.; Diekhöner, L.; Wahl, P.; Kern, K. *Phys. Rev. Lett.* **2002**, *88*, 096804.
- (16) Ujsaghy, O.; Kroha, J.; Szunyogh, L.; Zawadowski, A. *Phys. Rev. Lett.* **2000**, *85*, 2557.
- (17) Plihal, M.; Gadzuk, J. W. *Phys. Rev. B* **2001**, *63*, 085404.
- (18) Schrieffer, J. R.; Wol, P. A. *Phys. Rev.* **1966**, *149*, 491.
- (19) Govind, N.; Wang, Y. A.; Carter, E. A. *J. Chem. Phys.* **1999**, *110*, 7677.
- (20) Klüner, T.; Govind, N.; Wang, Y. A.; Carter, E. A. *Phys. Rev. Lett.* **2001**, *86*, 5954.
- (21) Klüner, T.; Govind, N.; Wang, Y. A.; Carter, E. A. *J. Chem. Phys.* **2002**, *116*, 42.
- (22) Segall, M. D.; Lindan, P. J. D.; Probert, M. J.; Pickard, C. J.; Hasnip, P. J.; Clark, S. J.; Payne, M. C. *J. Phys.: Condens. Matter* **2002**, *14*, 2717.
- (23) Perdew, J. P.; Zunger, A. *Phys. Rev. B* **1981**, *23*, 5048.
- (24) Laasonen, K.; Pasquarello, A.; Car, R.; Lee, C.; Vanderbilt, D. *Phys. Rev. B* **1993**, *47*, 10142.
- (25) Monkhorst, H. J.; Pack, J. D. *Phys. Rev. B* **1976**, *13*, 5188.
- (26) Karlström, G.; Lindh, R.; Malmqvist, P.-Å.; Roos, B. O.; Ryde, U.; Veryazov, V.; Widmark, P.-O.; Cossi, M.; Schimmelpfennig, B.; Neogrady, P.; Seijo, L. *Comput. Mater. Sci.* **2003**, *28*, 222.
- (27) Hay, P. J.; Wadt, W. R. *J. Chem. Phys.* **1985**, *82*, 270.
- (28) Roos, B. O. The multiconfigurational (MC) self-consistent field (SCF) theory. In *Lecture Notes in Quantum Chemistry*; Roos, B. O., Ed.; Springer-Verlag: Berlin, 1992; Vol. 58.
- (29) Siegbahn, P. E. M. The configuration interaction method. In *Lecture Notes in Quantum Chemistry*; Roos, B. O., Ed.; Springer-Verlag: Berlin, 1992; Vol. 58.

NL0602847